Radiometric Calibration of the EO-1 Advanced Land Imager

Jeffrey A. Mendenhall, Donald E. Lencioni, and Alexander C. Parker
Massachusetts Institute of Technology - Lincoln Laboratory
244 Wood Street, Lexington, MA 02420-9185
Tel. 781-981-0392, Fax 781-981-0969, e-mail: mendenhall@ll.mit.edu

ABSTRACT

The radiometric calibration of the Earth Observing 1 Advanced Land Imager (EO-1 ALI) was completed in the Spring of 1999 at Lincoln Laboratory. This calibration was conducted with the ALI as a fully assembled instrument in a thermal vacuum chamber at operational temperatures. The ALI was calibrated radiometrically at the system level from 0 to > 100% Earth-equivalent albedo using a combination of internal and external halogen and Xenon lamps attached to a large integrating sphere. Absolute radiometric calibration was achieved by measuring the output of the integrating sphere at each radiance level prior to ALI illumination using a NIST-traceable spectroradiometer. Additional radiometric characterization of this instrument was obtained from data collected using a collimator designed for the spectral calibration of the ALI. In this paper we review the techniques employed during radiometric calibration and present the measured gain, linearity, offset, signal-to-noise ratio and polarization sensitivity of each pixel. The testing results of a novel, in-flight solar calibration technique are also discussed. Finally, the results from a Lincoln Laboratory / Goddard Space Flight Center Landsat transfer radiometric study are presented.

Keywords: calibration, EO-1, radiometric, polarization, solar, land imager

1. INTRODUCTION

The Advanced Land Imager is a technology verification instrument and will fly on Earth Observing 1 - the first Earth observing satellite in NASA's New Millennium program (Figure 1, Lencioni and Hearn (1998), Digenis et al. (1998)). The ALI contains wide angle, pushbroom optics designed to provide a continuous 15° x 1.625° field of view without the use of a scan mirror. The focal plane for this instrument is partially populated with four sensor chip assemblies (SCA) and covers 3° by 1.625°. Each SCA contains 9 multispectral bands (30 meter resolution) and a single panchromatic band (10 meter resolution, Table 1). These bands have been designed to mimic six Landsat (Lauer et al., 1997) bands with three additional bands covering 0.433-0.453, 0.845-0.890, and 1.20-1.30 μm. The ALI is currently scheduled for launch on December 15, 1999 and will fly one minute behind Landsat-7 (launched April 15, 1999). In this configuration, both instruments will view identical scenes in order to verify the spatial, spectral, and radiometric performance of the ALI.

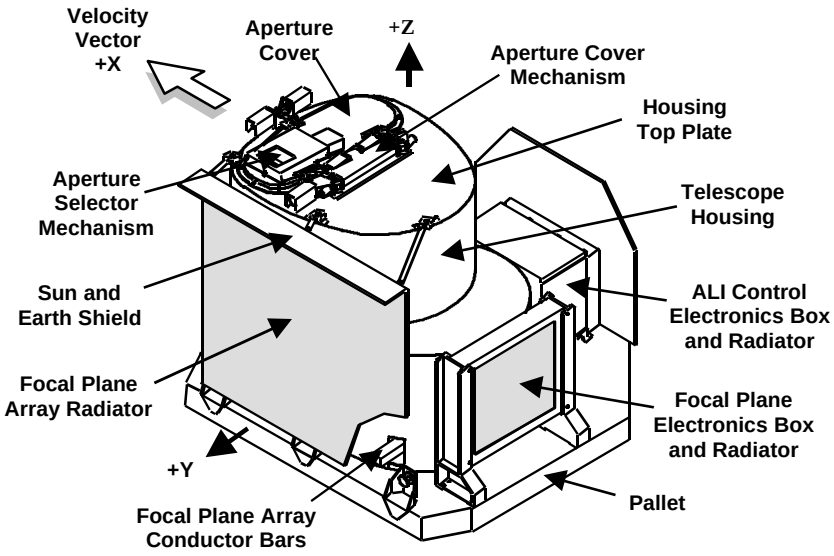

Figure 1: Earth Observing 1 Advanced Land Imager.

Band	Wavelength (μm)	Ground Sampling Distance (m)
Pan	0.48 – 0.69	10
MS-1'	0.433 – 0.453	30
MS-1	0.45 – 0.515	30
MS-2	0.525 – 0.605	30
MS-3	0.633 – 0.69	30
MS-4	0.775 – 0.805	30
MS-4'	0.845 – 0.89	30
MS-5'	1.2 – 1.3	30
MS-5	1.55 – 1.75	30
MS-7	2.08 – 2.35	30

Table 1: Spectral and spatial definitions for the ten EO-1 ALI bands.

Ground calibration of the Advanced Land Imager occurred from September 1998 through January 1999 at the Massachusetts Institute of Technology/Lincoln Laboratory. Included in this characterization period was the radiometric calibration of individual pixels at the system level. This paper provides a review of the techniques employed during radiometric calibration and the first results from the characterization of the gain, linearity, offset, and signal-to-noise ratio of each pixel. Additionally, polarization sensitivity of the instrument, a review of the data collected for verification of an in-flight solar calibration technique, and data collected as a part of the Landsat transfer radiometry program are discussed.

2. MEASUREMNT OF PIXEL GAIN, LINEARITY, OFFSET, AND SIGNAL-TO-NOISE RATIO

2.1 Technique

The technique we have adopted for the measurement of the gain, linearity, and offset for each ALI pixel consists of flooding the entrance aperture with a diffuse source of stable, broadband emission at various radiance levels and recording the output of the focal plane at each level. The source of diffuse emission is a 30-inch diameter integrating sphere with a 10-inch diameter output port manufactured by *Labsphere Inc*. (Figure 2). The sphere contains three internally mounted 150 Watt and one externally mounted 125 Watt halogen lamps. These lamps provide a combined radiance equal to 100% Earth-equivalent albedo for Bands 3, 4, 4p, 5p, 5, and 7 and the panchromatic band. Four additional externally mounted 300 Watt Xenon lamps were used to provide 100% Earth-equivalent albedo for Bands 1p, 1, and 2. Eight intermediate radiance levels from 0 to 100% Earth-equivalent albedo were obtained through a combination of sequentially extinguishing lamps and derating one internal lamp current. Exercising a linear attenuator mounted between the external halogen source and the integrating sphere provided an additional eight levels. This GPIB commanded slide provides up to 256 aperture variations for an externally mounted source. A similar attenuator is also located between one of the externally mounted Xenon source and the sphere to provide more flexibility in selecting radiance levels for Bands 1p, 1 and 2.

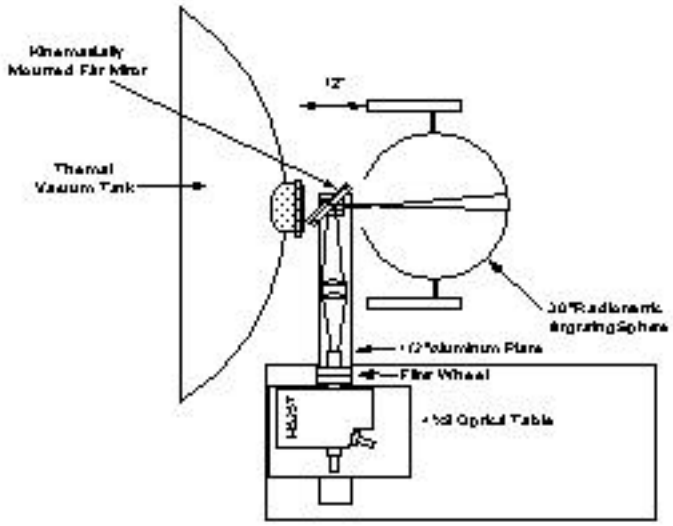

Figure 2: Integrating sphere and spectroradiometer used during radiometric calibration of the Advanced Land Imager.

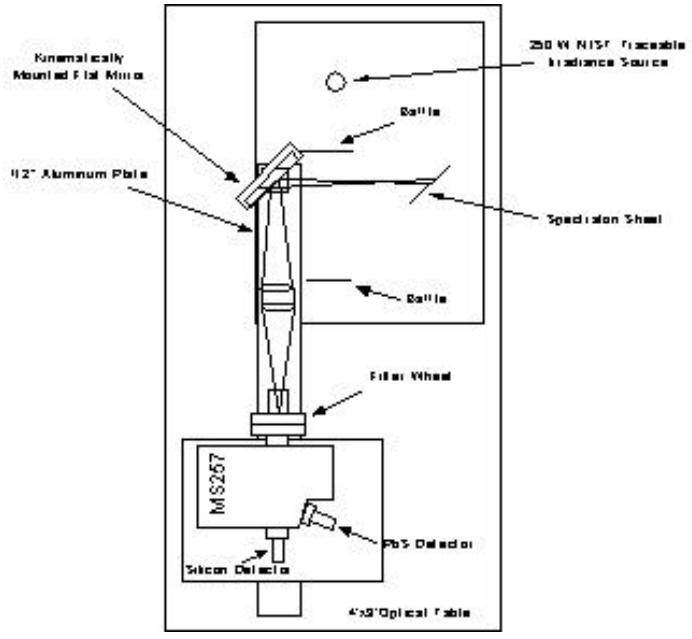

Figure 3: Radiometric transfer standard system built at Lincoln Laboratory. This system provides absolute radiometric traceability of the ALI to other sensors by iteratively scanning the NIST traceable 250 W halogen lamp and the large integrating sphere using the spectroradiometer.

2.2 Traceability to NIST

In order to provide absolute radiometric traceability to other sensors, a radiometric transfer standard system was constructed at Lincoln Laboratory (Figures 2 and 3). The principal components of the system are a NIST-traceable irradiance source and an *Oriel MS257* monochromator used as a spectroradiometer. The 250 Watt irradiance source is mounted on a post with proper baffling to control stray light from the room and reflections from the source off other surfaces. A standard radiance scene is generated by placing a *Labsphere Spectralon* (Leland and Arecchi, 1995) sheet 50 cm from the irradiance source. The monochromator field-of-view is limited to a 6.45 cm^2 region of the diffuse scene to maintain the traceability of the radiance source. A 6-inch flat mirror is placed between the *Spectralon* diffuser and entrance slit of the monochromator for convenient location of the source. Alternately scanning the radiance scene produced by the standard lamp and various radiance levels output by the large integrating sphere, radiometric NIST traceability is established for the EO-1 ALI. Additional near real-time monitoring of the sphere radiance level was accomplished by mounting the 6-inch flat mirror on a 12-inch post between the vacuum tank window and the integrating sphere. During radiometric calibration of the ALI, the mirror was removed and the response of the focal plane recorded. Between radiance levels, the mirror was kinematically mounted on the aluminum bar, redirecting a portion of the sphere radiance into the entrance slit of the spectroradiometer. The radiance of the integrating sphere was then measured from 300 to 2600 nm in 10 nm intervals with 5 nm FWHM resolution. Finally, continuous broadband monitoring of the sphere stability was provided by silicon and germanium detectors mechanically mounted to the sphere wall.

2.3 Data Collection

Radiometric data were collected in January, 1999 in a class 1,000 clean room at Lincoln Laboratory. This calibration was conducted with the ALI as a fully assembled instrument in a thermal vacuum chamber at operational temperatures.

Selection of the integrating sphere radiance level and monitoring of radiance stability was coordinated by the ALI Calibration Control Node (ACCN), a LabVIEW based personal computer operating on a Windows 95 platform. Commanding and housekeeping monitoring of the ALI was also controlled by the ACCN via a Goddard Space Flight Center provided RS2000 Advanced Spacecraft Integration and Systems Test (ASIST) computer. Data acquisition was performed by a Unix based Electrical Ground Support Equipment (EGSE1) computer. A Silicon Graphics Performance Assessment Machine (PAM) stored and processed focal plane data in real time for quick look assessment.

For each radiance level selected, the sphere was allowed to stabilize for one hour. A spectroradiometric scan of the sphere output from 300 – 2500 nm was then conducted after placing a six inch flat mirror between the sphere exit port and vacuum tank window to redirect the beam in to the monochromator. After the mirror was removed, the response of the focal plane was recorded for several integration periods (0.81, 1.35, 1.89, 2.97, 3.51, and 4.05 milliseconds). Finally, the ALI aperture cover was closed and reference dark frames recorded for identical integration periods.

Data were collected with the ALI illuminated by a combination of halogen sources only, a combination Xenon sources only, and a combination of halogen and Xenon sources. Additional data was collected using the halogen sources only with the focal plane operating at two other possible operating temperatures (215 K and 225 K) to assess the effects of temperature on focal plane response.

2.4 Analysis

The radiometric response of each pixel is a function of integration time and in-band radiance. Therefore, we begin our analysis by separately fitting each pixel's radiometric response (dn) as a function of integration time (ms) for a single sphere radiance level. Once this response is determined, the overall radiometric calibration for each pixel is greatly simplified. Applying the above fit, one may determine a pixel's response (dn) as a function of the product of in-band radiance and integration time (W ms /cm^2/sr). This response removes the requirement for separate calibration coefficients for each integration time. Rather, a pixel's in-band radiance for any operating configuration may be derived with knowledge of the pixel response (dn), calibration coefficient (W ms /cm^2/sr/dn) and integration time (ms)

$$R_P(W/cm^2/sr) = \frac{P_r(dn)C_P(W\ ms/cm^2/sr/dn)}{I(ms)}$$

Here, $\boldsymbol{R_p}$ is the in-band response for pixel $\boldsymbol{P}$, $\boldsymbol{P_r}$ is the digital response for pixel $\boldsymbol{P}$, $\boldsymbol{C_p}$ is the derived radiometric calibration coefficient, and $\boldsymbol{I}$ is the integration time of the focal plane at the time of the observation.

Prior to the radiometric characterization of each pixel, a final pixel-to-pixel correction is added to the model. First, a reference pixel is selected and fitted to the above model. However, during this analytical fit, each calculated in-band radiant output of the integrating sphere is allowed to vary by up to ±5%. This is done to reduce radiometric pixel-to-pixel variations (data scatter) to the single bit level while still remaining constrained by the ALI radiometric error budget. Radiance offsets derived from this fit are then applied to the remaining pixels during their radiometric characterizations.

2.5 Results

At this time have used the above algorithm and focal plane data collected during halogen lamp exposure only to derive a radiometric response coefficient as a function of the integration time (ms) and the product of in-band radiance and integration time (W ms /cm^2/sr) for each pixel of Band 3.

We find a second order polynomial provides the best fit of pixel response as a function of integration time. Figures 4 and 5 provide an example of linear and polynomial fits to the data for all pixels of Band 3. Although a linear fit to the data results in ± 1.0% errors between model and data for all integration times, a second order polynomial fit drives these errors to less that ± 0.4% for identical cases. Figure 6 provides a plot of nonlinearity versus integration time for pixel 100. Deviations from a linear response up to 1.5% are observed for higher integration times. Figure 7 depicts the nonlinearity of this fit for all pixels.

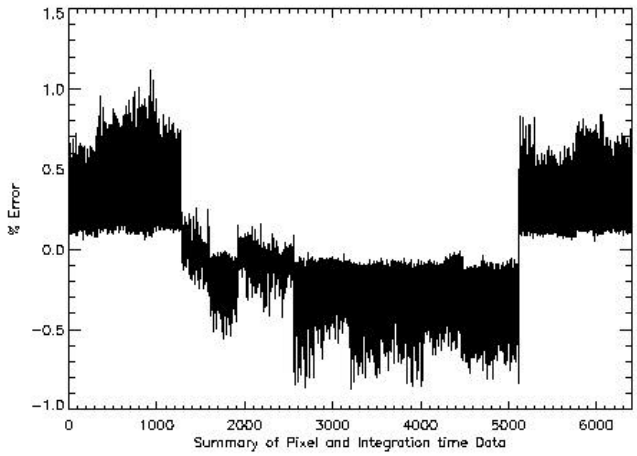

Figure 4: Summary of errors in linear fit of integration time data for Band 3. All pixels and all integration times are included in this plot.

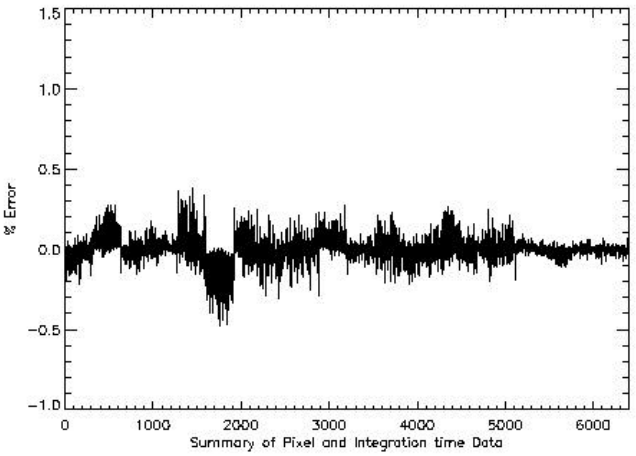

Figure 5: Summary of errors in polynomial fit of integration time data for Band 3. All pixels and all inegration times are included in this plot.

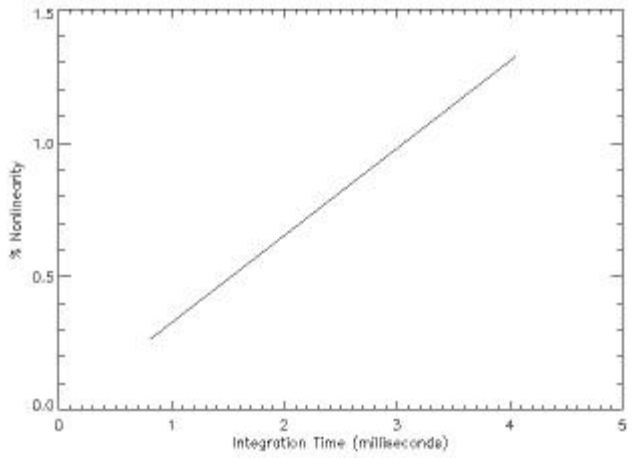

Figure 6: Nonlinearity of integration time fit for pixel 100, Band 3.

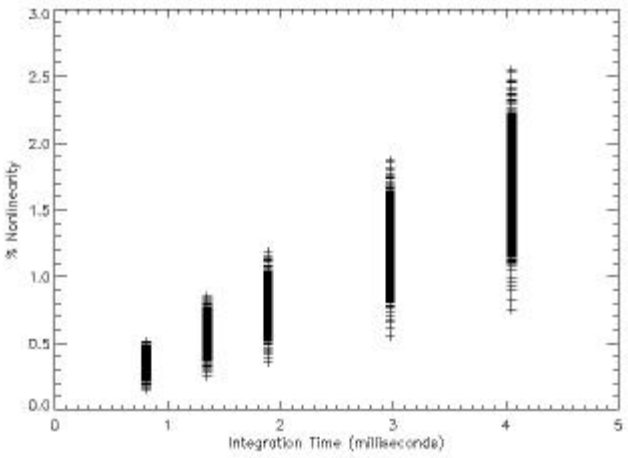

Figure 7: Nonlinearity of integration time fit for all pixels of Band 3.

The reference pixel selected for the calculation of in-band radiance offsets for pixel to pixel corrections was pixel 1. Allowing the calculated in-band radiant output of the integrating sphere to vary, linear and polynomial models were used to fit the data. From this fit we find in-band corrections to be less than 3.5% for all radiance levels. Using these factors as additive corrections to the model and applying the results from the radiometric fitting of data versus integration time, the radiometric characterization of all pixels in Band 3 was performed. We find the best fit of pixel response as a function of the product of radiance and integration time to also be a second order polynomial. Figures 8 and 9 provide an example of linear and polynomial fits to the data for all pixels of Band 3. Although a linear fit to the data results in ± 1-2% errors between model and data for all radiance levels, the polynomial fit drives these errors to less than ± 1% for 99% of all cases. Figure 10 provides a plot of nonlinearity versus the product of radiance and integration time for all pixels of Band 3. Figures 11 and 12 depict the offset and linear terms of this fit for all pixels. Figures 13 and 14 provide a graphic demonstration of the significant improvement in the residual error between model and data after the pixel to pixel radiometric correction is applied. For these fits, the residual error before the pixel to pixel correction is applied is reduced from ± 3-5% to ± 1% after the correction is applied. This pixel to pixel correction results in one out of twelve bit variations across the 3° field of view for uniform scenes (Figure 15).

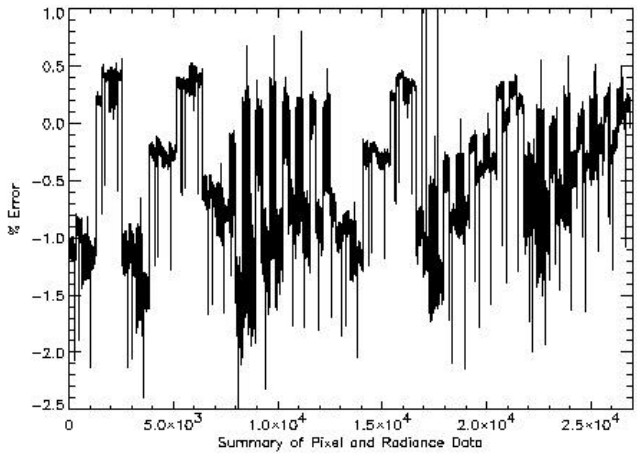

Figure 8: Summary of errors in linear fit of radiometric calibration data for Band 3. All pixels and all radiance-integration time products are included in this plot.

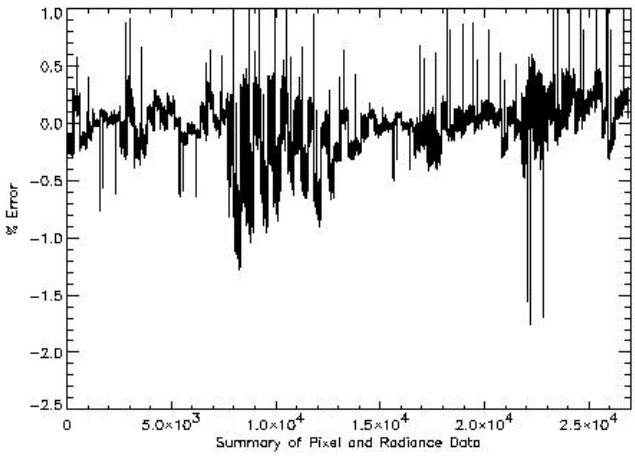

Figure 9: Summary of errors in polynominal fit of radiometric calibration data for Band 3. All pixels and all integration time products are included in this plot.

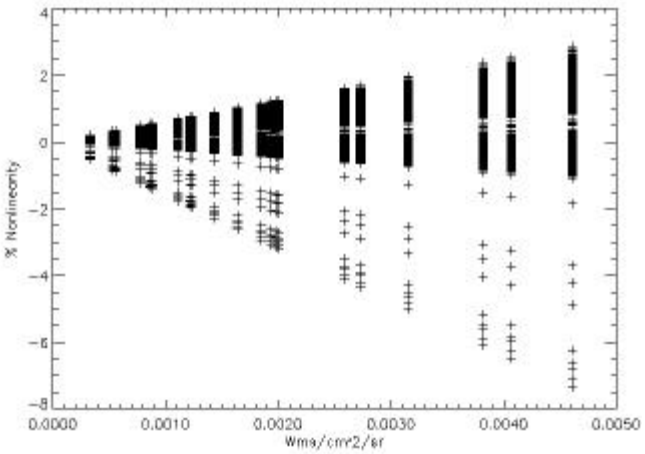

Figure 10: Nonlinearity of the product of radiance and integration time for all pixels of Band3. Eight pixels have nonlinearities greater than 2%.

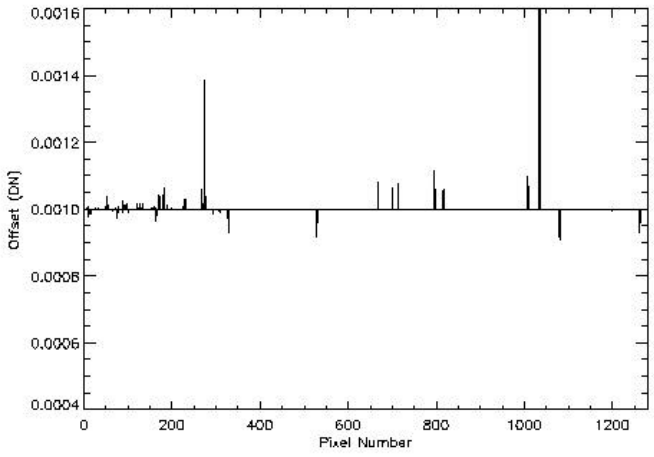

Figure 11: Offset values for polynomial fit to radiance-integration time product data for all pixels of Band 3.

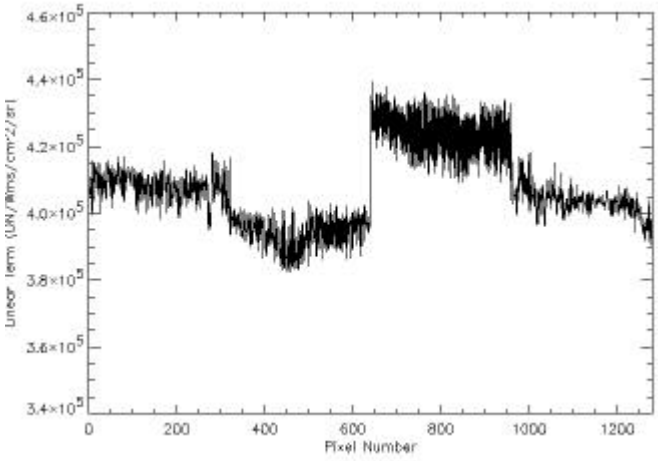

Figure 12: Linear term for polynomial fit to radiance-integration time product data for all pixels of Band 3.

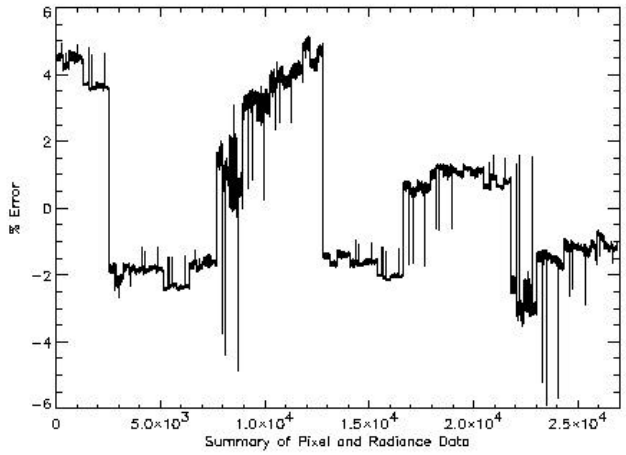

Figure 13: Summary of errors in radiometric data fit without pixel to pixel data corrections applied. All pixels in Band 3 and all radiance-integration time products are included in this plot.

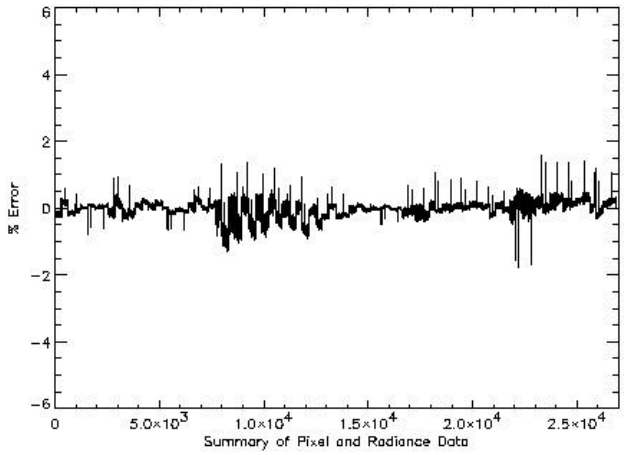

Figure 14: Summary of errors in radiometric data fit with pixel to pixel data corrections applied. All pixels in Band 3 and all radiance-integration time products are included in this plot.

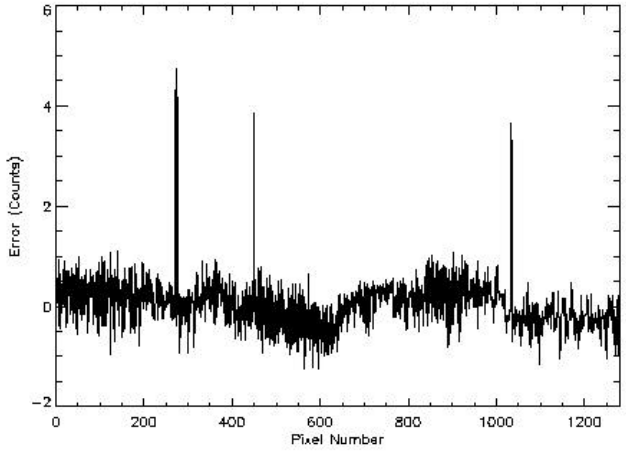

Figure 15: Example of Band 3 pixel to pixel variations for a uniform scene after radiometric calibration coefficients have been applied to the raw data. This data indicates only one out of twelve bit variations are expected across the 3° field of view for a uniform scene.

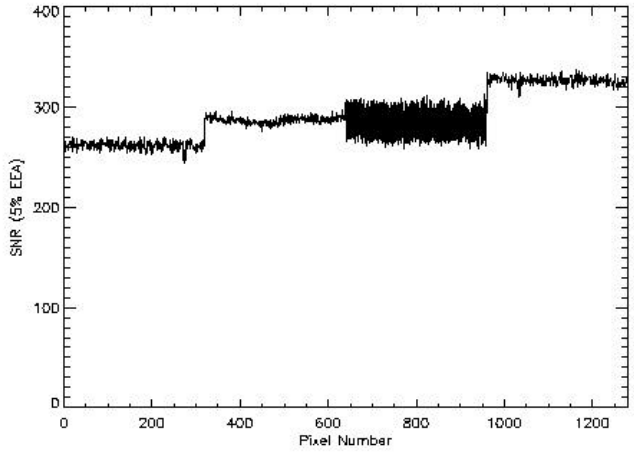

Figure 16: Calculated signal to noise ratio for all pixels of Band 3 for a 5% Earth equivalent albedo (EEV) radiance level. Ratios were obtained by fitting signal to noise data obtained during radiometric calibration of the Advanced Land Imager.

Finally, detector signal to noise ratios have been derived from the above analysis. Using the radiometric calibration in-band radiance ($W/cm^2/sr$) and detector response and standard deviation (dn) data, a signal to noise ratio as a function of radiance fit may also be performed. From this, a predicted signal-to-noise ratio for any pixel may be calculated for any radiance level. Figure 16 depicts the signal-to-noise ratio (260-330) for 5% Earth-equivalent albedo for all pixels in Band 3. These values are in good agreement with the signal to noise ratios calculated from subsystem measurements.

3. POLARIZATION SENSITIVITY

3.1 Technique

The ALI polarization sensitivity was tested by flooding the entrance aperture with a diffuse source of stable, narrowband emission at various linear polarization angles and recording the output of the focal plane at each angle. The collimator used for this test was identical to the collimator used during spectral calibration with the addition of two Glan-Thompson polarizing prisms (Figure 17). A monochromator was used to select a narrow portion of the spectrum for the band of interest. For this test, a bandwidth of 4 nm centered at each ALI multispectral band was used. A Glan-Thompson polarizer was placed at the exit port of the monocrhomator to allow the user to select the angle of polarization throughout the test. An off-axis parabola collimated the beam and a turning flat was used to direct the beam into the vacuum chamber. Finally, a second polarizer and detector (silicon for VNIR bands and lead-sulfide for SWIR bands) was mounted in front of the vacuum tank window between ALI measurements to determine the final polarization of the beam entering the vacuum tank window. This was done to monitor any additional polarization effects induced by the parabola and turning mirrors.

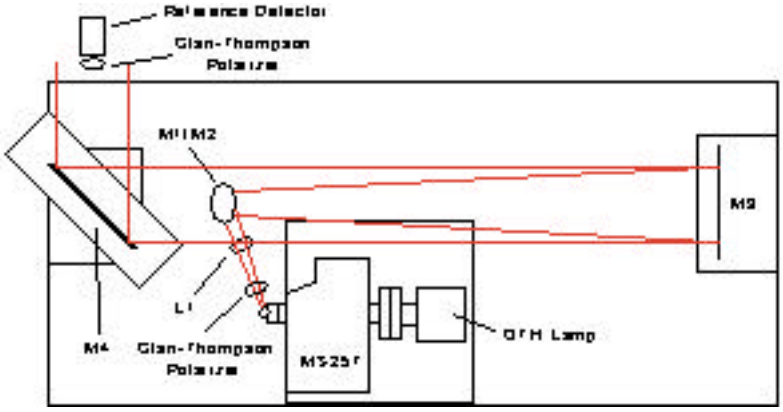

Figure 17: Calibration setup for the evaluation of the polarization sensitivity of the ALI.

Polarization data were collected with the collimated beam's spectrum centered on each of the VNIR and SWIR bands. Panchromatic data were also collected at several wavelengths within the band's spectral response. For each spectral band, data was collected for 0, 30, 60, 90, 120,150, and 180 degrees of polarization. Measurements using the second polarizer and reference detector were made at 0, 30, 60, 90, 120, 150, and 180 degrees of polarization prior to each ALI data collection event.

3.2 Analysis

The ALI polarization sensitivity is determined by comparing focal plane response as a function of polarization angle. First, all focal plane data are background subtracted. The data from each band is then normalized to unity for the zero degree polarization case. The actual polarization angle of the beam for each data set is derived from the reference detector viewing the beam in front of the turning flat. Applying the above corrections to the original polarization angle data, a corrected pixel response versus polarization angle is created. Qualitative insight into the polarization sensitivity of the ALI may then be obtained by plotting the response of the ALI versus polarization angle for each band in polar coordinates (e.g. Figure 18). Quantitatively, the `degree of polarization' of the ALI for any band has been calculated as

$$P_B = \frac{T_{2B} - T_{1B}}{T_{1B} + T_{2B}}$$

Here, P_B is the ALI polarization sensitivity for band B, T_1 is the minimum focal plane response, and T_2 is the maximum focal plane response.

3.3 Results

Polarization characterization of the ALI is currently under development. However, Figure 18 provides an indication of the polarization sensitivity of pixel 800, Band 1p. In this figure, the dark corrected detector pixel response has been normalized to unity at 0° linear polarization. For a polarization insensitive instrument, the response as a function of polarization angle, plotted in polar coordinates, would form a perfect circle of radius = 1. However, we calculate for pixel 800, Band 1p, the polarization sensitivity to be 4% for the ALI.

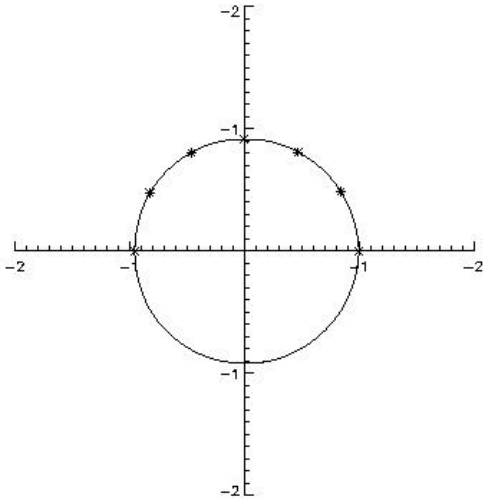

Figure 18: ALI focal plane response to linearly polarized radiation for pixel 800, Band 1p. The data have been normalized to unity at 0° polarization. Asterices indicate measured data points. All other values are interpolated.

4. VERIFICATION OF AN IN-FLIGHT SOLAR CALIBRATION TECHNIQUE

4.1 Solar Calibration Technique

As a part of the in-flight radiometric calibration plan (Mendenhall et al., 1998), periodically, the instrument aperture cover will be closed, a *Labsphere* space-grade *Spectralon* diffuser will be placed in front of the ALI M2 mirror, and the instrument pointed in the direction of the Sun. After a brief stabilization period, a slide is withdrawn at a constant velocity, to expose a slotted mask (Figure 19), filling a portion of the aperture cover. This mask contains seven reference slots designed to provide a piecewise linear increase (decrease) of signal level from 0% to 90% equivalent diffuse Earth reflectance. As the slide is withdrawn, the solar flux entering through the exposed slot(s) will be diffusely scattered off the Lambertian *Spectralon* reflector, producing uniform scenes of incrementing radiance. Reference bars, located between the slots will provide a constant signal level for 0.5 seconds for each radiance level. Periodic absolute radiometric calibration of the focal plane will be maintained by recording the output of the focal plane as a function of calibration mask position (assuming a known solar irradiance from 400-2500 nm and a stable *Spectralon* diffuser).

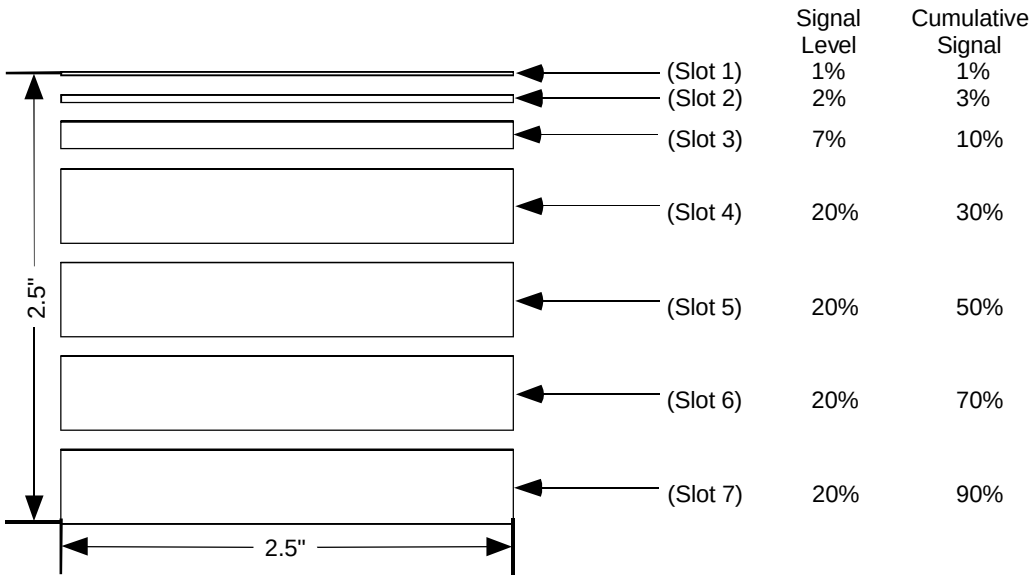

Figure 19: Aperture cover mask used during solar calibration

4.2 Verification Method

The solar calibration validation technique centers on the accurate prediction of aperture selector throughput based on an accurately known reflectance standard. The collimator used during solar calibration validation was the same used for spectral calibration. The focused beam from a 1000 watt Xenon source was placed near the focus of a 17-inch diameter off-axis parabola. The collimated beam is then reflected off a 18-inch flat mirror and into the entrance aperture of the instrument.

Solar calibration verification data were collected as a part of the radiometric calibration of the ALI in January, 1999. Initially, the kilowatt Xenon source was turned on and allowed to stabilize for one hour. Data was then collected by the ALI with a large *Spectralon* panel covering the 17" diameter flat mirror directing the beam into the vacuum tank window. In this configuration the aperture cover was open and solar diffuser stowed. This data serves as the baseline for ALI solar calibration verification. Next, the aperture cover was closed, the *Spectralon* diffuser removed and data collected by the ALI using the solar calibration technique described above. A broadband silicon detector was used to monitor the beam stability before, between, and after the two data collection periods. We find the beam to be stable to within 1.5% during this time.

4.3 Analysis

Once the two data sets have been collected, an expected focal plane response when the *Spectralon* panel was covering M4 is calculated based on the solar calibration measurement. The expected focal plane response has been calculated as

$$F_E(dn) = \frac{Max(F_{SC})(dn)}{0.9\cos(45^\circ)\,0.99}.$$

Here, $\boldsymbol{F_E}$ is the expected focal plane response and $\boldsymbol{Max(F_{sc})}$ is the maximum recorded focal plane response using the solar calibration technique. The cosine factor accounts for the placement of the *Spectralon* diffuser relative to the beam, the 0.9 factor accounts for the expected percentage of the incident beam using this technique, and 0.99 is the accepted reflectivity of the Spectralon panel at 1.0 μ. In this calculation, the spectrum and intensity of the laboratory source cancel out, so no knowledge of the source is required. Finally, once the expected focal plane response has been calculated, it is compared to the measured response to validate the calibration technique.

4.4 Results

Analysis of solar calibration data is currently in progress. Figure 20 depicts the background subtracted data for a single solar calibration data collection event for pixel 100, Band 3. The staircase shape of the data is the result of the aperture selector initially retracting and then covering an increasing number of slots behind the calibration slide. Normalizing the flux incident on the focal plane to be one when all of the slots are exposed, we find the data during stable periods when the aperture selector is between slots to be 1.1, 1.8, 6.9, 21.5, 22.6, 23.3, and 22.8% of the maximum response respectively. This result closely matches that predicted by the solar calibration technique.

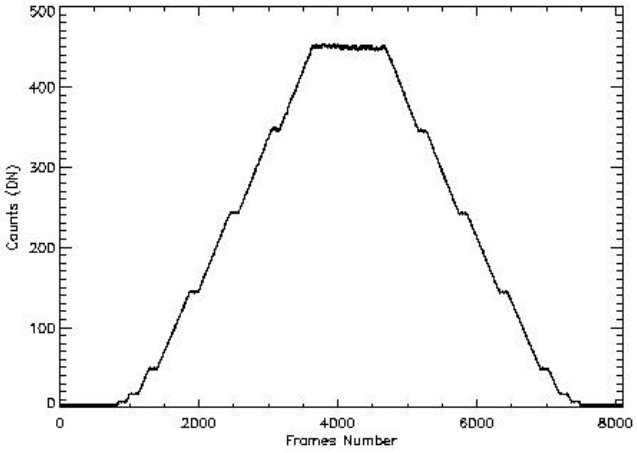

Figure 20: Data collected using solar calibration technique. The staircase shape of the data is the result of the aperture selector initially retracting and then covering an increasing number of slots behind the calibration slide.

5. LANDSAT TRANSFER RADIOMETER STUDY

5.1 Technique

The Landsat Transfer Radiometer (LXR) was used to measure the output intensity of the integrating sphere at Lincoln Laboratory for several spectral bands and several radiance levels. The LXR is a portable Goddard Space Flight Center six channel filter radiometer (Markham et al. 1998). Behind each ion assist deposited filter is a single silicon photodiode that views the integrating sphere output port simultaneously. Four of the six channel filters have been cut from the same substrate as those from the Landsat 7 ETM+. As a result these closely match the Landsat VNIR bands 1-4. The remaining two bands are 10 nm wide and are centered at 441 nm and 662 nm respectively. The spectral coverage for all LXR bands is provided in Table 2. This instrument is used by GSFC to measure the in-band radiance of calibration sources across the country in order to provide a common radiometric tie between independently calibrated VNIR sensitive instruments. LXR measurements at Lincoln Laboratory were collected in series with spectroradiometric measurements for each sphere level selected. Spectroradiometric data were then rebinned to match the spectral bands of the LXR and the results compared.

Band	Wavelength (μm)	Equivalent Landsat Band
5	0.435 – 0.445	---
1	0.45 – 0.515	1
2	0.525 – 0.605	2
6	0.657 – 0.665	---
3	0.633 – 0.69	3
4	0.775 – 0.805	4

Table 2: Spectral definitions for the Landsat Transfer Radiometer bands.

5.2 Data Collection

Data were collected by the Landsat Transfer Radiometer and spectroradiometer at Lincoln Laboratory in August of 1998. Twelve halogen and four Xenon radiance levels were selected for this study. A total of four data runs were performed during this period. First, data were collected by the LXR and spectroradiometer viewing the integrating sphere directly. Next, data were collected by the LXR and spectroradiometer viewing the integrating sphere through the vacuum tank window that was used during ALI calibration. Finally, data collection with the LXR was repeated in order to ascertain the repeatability and stability of the LXR and the integrating sphere.

5.3 Analysis

Data analysis of LXR and spectroradiometric data was performed independently at Goddard Space Flight Center and Lincoln Laboratory respectively. Absolute in-band radiances for the LXR were provided by GSFC based on NIST traceable calibration of the instrument. In order to compare spectroradiometric data with LXR data, spectroradiometric data were normalized and integrated over the LXR spectral bands. First, NIST traceable calibration corrections were applied to the spectroradiometric data to place these measurements on an absolute scale. Interpolated, absolute radiance measurements were then normalized by the LXR spectral transmission curve for each band. Each normalized band data is then integrated and divided by the integrated relative spectral response of the LXR or

$$L(c,s) = \frac{\int RSR(c,\boldsymbol{l}) L_{\boldsymbol{l}}(s,\boldsymbol{l}) d\boldsymbol{l}}{\int RSR(c,\boldsymbol{l}) d\boldsymbol{l}}.$$

Here, $L(c,s)$ is the calculated relative spectral response weighted spectral radiance for band c and sphere level s, $RSR(c, \boldsymbol{l})$ is the LXR relative spectral response for band c, and $L_{\boldsymbol{l}}(s, \boldsymbol{l})$ is the spectroradiometrically measured spectral radiance of the MIT/Lincoln Laboratory integrating sphere for level s. Units for this comparison are $mW/cm^2/sr/\mu$.

5.4 Results

At this time, a comparison of LXR and spectroradiometric measurements has been performed for data collected when only halogen lamps were active in the sphere. The results from LXR measurements and calculated LXR in-band radiance estimates based on spectroradiometric measurements of the MIT/Lincoln Laboratory integrating sphere are provided in Table 3. For all levels and all bands we find LXR measurements to agree with spectroradiometric measurements to within 5%. These measurements provide confidence in the usefulness of the LXR as a transfer radiometer for a variety of missions that include VNIR arrays. Additionally, this agreement indicates the radiance estimates of the integrating sphere used during radiometric calibration of the Advanced Land Imager are within the prescribed 5% error budget.

Radiance Level		LXR Band 5	LXR Band 1	LXR Band 2	LXR Band 6	LXR Band 3	LXR Band 4
1	LXR	12.55	21.47	42.94	68.85	68.77	90.91
	SPECTRORAD	12.03	20.74	41.19	66.64	66.83	90.07
	SPECTRORAD/LXR	95.9	96.6	95.9	96.8	97.2	99.1
2	LXR	10.79	18.60	37.53	60.59	60.53	80.32
	SPECTRORAD	10.30	17.88	35.84	58.48	58.56	79.55
	SPECTRORAD/LXR	95.5	96.1	95.5	96.5	96.7	99.0
3	LXR	8.97	15.30	30.53	48.83	48.78	64.40
	SPECTRORAD	8.56	14.69	29.13	47.00	47.16	63.37
	SPECTRORAD/LXR	95.4	96.0	95.4	96.3	96.7	98.4
4	LXR	7.23	12.48	25.17	40.68	40.61	53.94
	SPECTRORAD	6.88	11.95	23.93	38.93	39.12	53.07
	SPECTRORAD/LXR	95.2	95.8	95.1	95.7	96.3	98.4
5	LXR	5.14	8.74	17.38	27.76	27.73	36.67
	SPECTRORAD	4.85	8.30	16.38	26.36	26.48	35.80
	SPECTRORAD/LXR	94.5	95.0	94.2	95.0	95.5	97.6
6	LXR	3.42	5.94	12.09	19.66	19.64	26.27
	SPECTRORAD	3.19	5.56	11.22	18.43	18.48	25.49
	SPECTRORAD/LXR	93.2	93.6	92.8	93.8	94.1	97.0
7	LXR	1.74	2.82	5.35	8.16	8.17	10.48
	SPECTRORAD	1.66	2.72	5.12	7.88	7.91	10.38
	SPECTRORAD/LXR	95.4	96.6	95.6	96.6	96.8	99.0

Table3: Landsat Transfer Radiometer study results. LXR and spectroradiometrically derived in-band measurements are listed for seven halogen radiance settings of the Lincoln Laboratory integrating sphere. Units for in-band measurements are $mW/cm^2/sr/\mu$.

6. DISCUSSION

A wealth of radiometric calibration data has been obtained for the EO-1 Advanced Land Imager. Initial results for Band 3 indicate the calibration data collected and analysis techniques adopted for ALI calibration are valid. Advances in radiometric calibration analysis have made it possible to obtain a single set of calibration coefficients applicable for any focal plane integration time and radiance level. Calculated signal-to-noise ratios are within 10% of the estimated values for Band 3. These high signal to noise ratios highlight a key advantage of push-broom optics over wisk-broom optics and should be invaluable for low illumination scenes. Finally, work is underway to expand the analysis of radiometric calibration data to include all bands, further understand the polarization sensitivity of this instrument, and validate the on-board solar calibration technique of the Advanced Land Imager.

7. ACKNOWLEDGEMENTS

The authors wish to thank the following individuals of MIT Lincoln Laboratory: Mr. Patrick Quinn for his assistance in building and testing the radiometric transfer standard and collecting data in the laboratory, Mr. Eric Ringdahl for his technical assistance in the laboratory, and Miss Shalini Agarwal for her assistance in reducing the polarization sensitivity data.

This work was sponsored by NASA/Goddard Space Flight Center under U.S. Air Force Contract number F19628-95-C-0002.

Opinions, interpretations, conclusions, and recommendations are those of the author and are not necessarily endorsed by the United States Air Force.

8. REFERENCES

Digenis, C. J., Lencioni, D. E., and Bicknell, W. E., Proc. SPIE, **3439,** 49, 1998.

Lauer, D. T., Morain, S. A., and Salamonson, V. V., Photogramm. Eng. and Remote Sens., **6**, 831, 1997.

Leland, J. E., Arecchi, A. V., Proc. SPIE, **2475**, p. 384, 1995.

Lencioni, D. E., and Hearn, D. R., "New Millennium EO-1 Advanced Land Imager", *International Symposium on Spectral Sensing Research,* San Diego, Dec. 13-19, 1997, Int. Soc. For Photogrammetry & Remote Sensing, 1998.

Lencioni, D. E., Hearn, D. R., Mendenhall, J. A., and Bicknell, W. E., This conference, paper number [3750-12], 1999.

Markham, B. L., Schafer, J. S., Wood Jr., F. M., Dabney, P. W., Barker, J. L., Metrologi, **35**, p. 643, 1998.

Mendenhall, J. A., Lencioni, D. E, Hearn, D. R., and Parker, A. C., Proc. SPIE, **3439**, 390, 1998.